## JOURNAL OF MARINE RESEARCH

The *Journal of Marine Research,* one of the oldest journals in American marine science, published important peer-reviewed original research on a broad array of topics in physical, biological, and chemical oceanography vital to the academic oceanographic community in the long and rich tradition of the Sears Foundation for Marine Research at Yale University.

An archive of all issues from 1937 to 2021 (Volume 1–79) are available through EliScholar, a digital platform for scholarly publishing provided by Yale University Library at https://elischolar.library.yale.edu/.

Requests for permission to clear rights for use of this content should be directed to the authors, their estates, or other representatives. The *Journal of Marine Research* has no contact information beyond the affiliations listed in the published articles. We ask that you provide attribution to the *Journal of Marine Research.*

Yale University provides access to these materials for educational and research purposes only. Copyright or other proprietary rights to content contained in this document may be held by individuals or entities other than, or in addition to, Yale University. You are solely responsible for determining the ownership of the copyright, and for obtaining permission for your intended use. Yale University makes no warranty that your distribution, reproduction, or other use of these materials will not infringe the rights of third parties.

# A field study of wave-induced pressure fluctuations above surface gravity waves[1]

R. L. Snyder

*Nova University*
*Physical Oceanographic Laboratory*
*8000 North Ocean Drive*
*Dania, Florida 33004, U.S.A.*

## ABSTRACT

The atmospheric pressure field above waves was monitored at two experimental sites in the Bight of Abaco (BOA), Bahamas, using horizontal arrays of up to four microbarographs and four wave recorders. During four separate field experiments in the period June 1968– April 1972, 96 hours of data were obtained. These data cover a wind-speed range of 3–10 m/s and a microbarograph elevation range (relative to the mean surface) of 0.5–2.0 m. The atmospheric pressure spectra typically show a wave-induced peak 5–20 times background, but the coherence between atmospheric pressure and surface elevation is low. The relative phases between microbarographs indicate that the background fluctuations have the dispersion of "frozen" turbulence, while the peak fluctuations have the dispersion of surface gravity waves. For a significant portion of the data, the dominant peak fluctuation is associated with surface gravity waves traveling against the wind. Reflection from the laboratory vessel accounts for most, but not all, observations of such waves.

Analysis of the wave-coherent portion of the atmospheric pressure fluctuation supports the conclusion that the phase of the pressure associated with a given wave component is constant with elevation and that its amplitude decays exponentially from the mean surface, in substantial agreement with Elliott (1972). The decay parameter is essentially that predicted by linear potential theory. Consistent with this conclusion, the microbarograph data were extrapolated to the mean surface, and wave growth rates were estimated from a directional cross-spectrum analysis. The implied growth rates are roughly one-tenth as large as those observed by Dobson (1971) and one-half as large as those observed by Elliott (1972). These rates are comparable with the predictions of the Miles (1957) theory; they are not nearly large enough to account for existing field observations of wave growth. This conclusion is contrary to that of Dobson (1971), but it is consistent with the conclusion of K. Hasselmann *et al* (1973), in the JONSWAP experiment, that wave components on the low-frequency face of the spectrum grow primarily as the result of nonlinear interactions. The integral momentum transfer from the atmosphere to waves, over a limited range of frequencies encompassing the spectral peak, is only several percent of the estimated stress associated with the mean air flow. Evidence is presented that waves traveling faster than the wind or against the wind are damped.

Fits to the observed wave spectra using the JONSWAP spectral form yield spectral para-

meters for the May 1970 BOA spectra which are, despite the different fetch distribution, remarkably consistent with those for the JONSWAP spectra. Only the Phillips (1958) parameter differs significantly; it is roughly half as large for these spectra as for JONSWAP. The implied nonlinear momentum transfer for the May 1970 BOA spectra is roughly one-sixth that of JONSWAP. The integral momentum transfer from the atmosphere to the JONSWAP wave field implied by the present study is consistent with the overall momentum balance as discussed by K. Hasselmann *et al* (1973). This transfer is smaller than the total stress but is adequate to provide the momentum required by the evolving wave field. The estimated transfer may account for several features of the JONSWAP plot of the Phillips parameter.

## 1. Introduction

The wind generation of surface gravity waves in deep water is thought to be governed by an equation first proposed by K. Hasselmann (1960):

$$\frac{\partial}{\partial t} F_{\zeta^2} + V(k) \cdot \nabla F_{\zeta^2} = \alpha + \beta F_{\zeta^2} + N_1 + N_2 + \ldots, \qquad (1)$$

where

$F_{\zeta^2}(x,t,k)$ is the spectral intensity of a wave component with propagation vector $k$ at horizontal position $x$ and time $t$; $V(k) \equiv \nabla_k \omega(k)$ is the group velocity for the $k$ component (with radial frequency $\omega(k)$);

$\alpha$ is the rate of change of $F_{\zeta^2}$ resulting from turbulent atmospheric pressure fluctuations (Phillips, 1957);

$\beta F_{\zeta^2}$ is the rate of change of $F_{\zeta^2}$ resulting from the shear instability of the mean air flow (Miles, 1957);

$N_1$ is the rate of change of $F_{\zeta^2}$ resulting from weak nonlinear interactions between wave components (K. Hasselmann, 1962); and

$N_2$ is the rate of change of $F_{\zeta^2}$ resulting from whitecapping.

Attempts to monitor various terms of this equation in the laboratory and in the field have included:

a. *Longuett-Higgins, Cartwright, and Smith* (1963). Observations of atmospheric pressure from a floating buoy allowed several qualitative conclusions regarding the first two terms on the right-hand side of (1). The observed pressure was highly coherent with surface elevation (probably owing to the hydrostatic contribution) and had a magnitude consistent with Miles' (1957) theory. The phase was not established with sufficient accuracy to provide a reliable estimate of energy or momentum transfer.

b. *Snyder and Cox* (1966). Using a towed directional array of wave recorders, the left-hand side of (1) was monitored in the field for a single wave component (17 m) for wind speeds between 5 and 10 m/s. The observed growth was consistent with a linearized version of (1) with $\alpha$ predicted by Phillips'

(1957) theory, assuming the turbulent atmospheric pressure spectrum to be comparable with that measured over land by Priestley (1965). $\beta$, however, was of order

$$\beta \sim s(\boldsymbol{k} \cdot \boldsymbol{W} - \omega(k)), \tag{2}$$

where $\boldsymbol{W}$ is a suitably chosen wind velocity and $s$ is the ratio of the density of air to that of water. (2) is one order of magnitude larger than predicted by Miles' (1957) theory. An extrapolation of (2) to other wave components furnished an estimate of the momentum flux to waves several times larger than the stress associated with the mean flow.

c. *Barnett and Wilkerson* (1967). Analysis of an aircraft-mounted radar altimeter record obtained off the coast of Maryland yielded wave growth observations for a full range of wave components at a single wind speed. The observed growth was consistent with a linear version of (1), with $\beta$ given approximately by (2). However, turbulent pressures were required to be 50 times as energetic as those extrapolated from Priestley's (1965) measurements, in order to account for $\alpha$. A significant tendency for wave components to overshoot their equilibrium value was observed.

d. *Shemdin* (1969). Laboratory studies of wave-induced pressure and velocity above surface gravity waves yielded energy and momentum transfers to waves of the same order as predicted by Miles (1957) when

$$\frac{\boldsymbol{k} \cdot \boldsymbol{W}}{\omega(k)} > 4,$$

but somewhat larger than the Miles prediction when

$$2 < \frac{\boldsymbol{k} \cdot \boldsymbol{W}}{\omega(k)} < 4.$$

e. *Dobson* (1971). Field measurements of atmospheric pressure above surface gravity waves were obtained using a buoy-mounted pressure sensor riding on a staff. The phase of the observed pressure differed from the Miles (1957) prediction by 20°, and the resulting energy transfer was comparable with (2). The total momentum flux was comparable to the stress associated with the mean flow.

f. *Elliott* (1972). Field measurements of atmospheric pressure above waves were obtained using a vertical array of fixed pressure sensors. The pressure spectra exhibited a large wave-induced peak. The data were consistent with a wave-coherent pressure field which decays quasi-exponentially (the decay parameter was found to depend on the wind speed) without change of phase from the mean surface. The energy transfer was approximately one-fifth of (2).

g. K. Hasselmann, Barnett, Bouws, Carlson, Cartwright, Enke, Ewing, Gienapp, D. Hasselmann, Krusemann, Meerburg, Müller, Olbers, Richter, Sell, and Walden (1973). A major experiment to monitor the left-hand side and nonlinear source term $N_1$ for (1) (computed from the spectrum of surface elevation using K. Hasselmann's (1962) theory) was conducted in the North Sea (JONSWAP). The spectrum was observed to evolve in "self similar" fashion, and to be parameterized by a suitable non-dimensional fetch. Nonlinear interactions were found to dominate the growth mechanism on the forward slope of the spectrum, and to explain in qualitative terms (a) the shape and evolution of the spectrum, and (b) the wind stress "paradox" associated with the large exponential growth observed by both Snyder and Cox (1966) and Barnett and Wilkerson (1967). The resulting minimum momentum transfer to waves resulting from the atmospheric interaction was estimated from (1) to be approximately 20% of the wind stress, assuming $N_2$ to be small across the significant range of the wave spectrum.

The experiments described in this paper were conceived, like those of Dobson and Elliott, as an attempt to determine to what extent wave-coherent fluctuations of atmospheric pressure can account for observed wave growth. To simplify the field observations, a fixed instrumentation was developed; in order to look at the directional characteristics of the atmospheric pressure field, a horizontal array of instruments was employed.

## 2. Field experiments in the Bight of Abaco (BOA)

The data were obtained in four separate field experiments, listed in Table I. The two sites are shown in Figure 1. The microbarographs and their installation at Site 1 are described in a companion paper (Snyder *et al*, 1973). The microbarographs and the wave recorders (Snodgrass Mark X pressure transducers) were supported by 6-cm diameter pipe stands resting on the bottom. The microbarograph probes were fixed vertically 0.5–2 m above the mean surface. At Site 1, tide elevation and wind velocity (nominally at 5 m above the mean surface) were monitored from a nearby tower. Wind velocity also was monitored during the May 1970 experiment at a somewhat lower elevation. The tide signal was used to determine all instrument elevations relative to the

Table I. Experiment parameters.

| Date | Site | NW | NM | NA | Hours | Remarks |
|---|---|---|---|---|---|---|
| June 1968 . . . . . . . . | 1 | 4 | 4 | 1 | 16 | Preliminary experiment |
| May 1970 . . . . . . . . . | 1 | 4 | 4 | 2 | 48 | Main experiment |
| December 1970 . . . . | 2 | 1 | 3 | 1 | 9 | Auxiliary experiment |
| April 1972 . . . . . . . . | 1 | 4 | 3 | 1 | 23 | Auxiliary experiment |

NW – number of wave recorders
NM – number of microbarographs
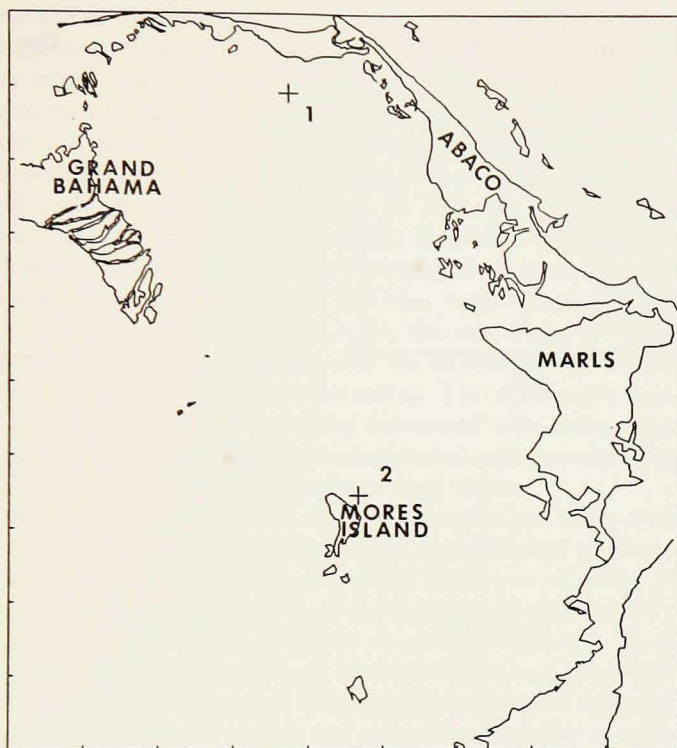NA – number of anemometers

Figure 1. The Bight of Abaco, showing site locations for the field experiments. Marls is a mangrove swamp.
Scale is 10 km per division. Mean depth is 7.3 m at Site 1, 3.1 m at Site 2.

mean surface (within 3 cm). All signals were returned by cable to a vessel moored at a distance of 125 m and recorded serially using a 16-channel data-acquisition system.

The instrument configurations for the four experiments are shown in Figure 2. Instrument spacing for the initial configuration proved somewhat large for the easterly winds encountered during the May 1970 experiment. This configuration was modified accordingly in April 1972. The close spacing and the reduced number of instruments for the December 1970 experiment were a result of the limited objectives for this experiment.

Historically, the first of the experiments in June 1968 provided a test of the instrumentation and experimental design but yielded insufficient data upon which to base any firm conclusions. The main experiment in May 1970 produced considerable data, the analysis of which revealed that the atmospheric pressure signals were highly coherent with phase differences characteristic of either (1) upwind-traveling surface gravity waves, or (2) downwind-traveling
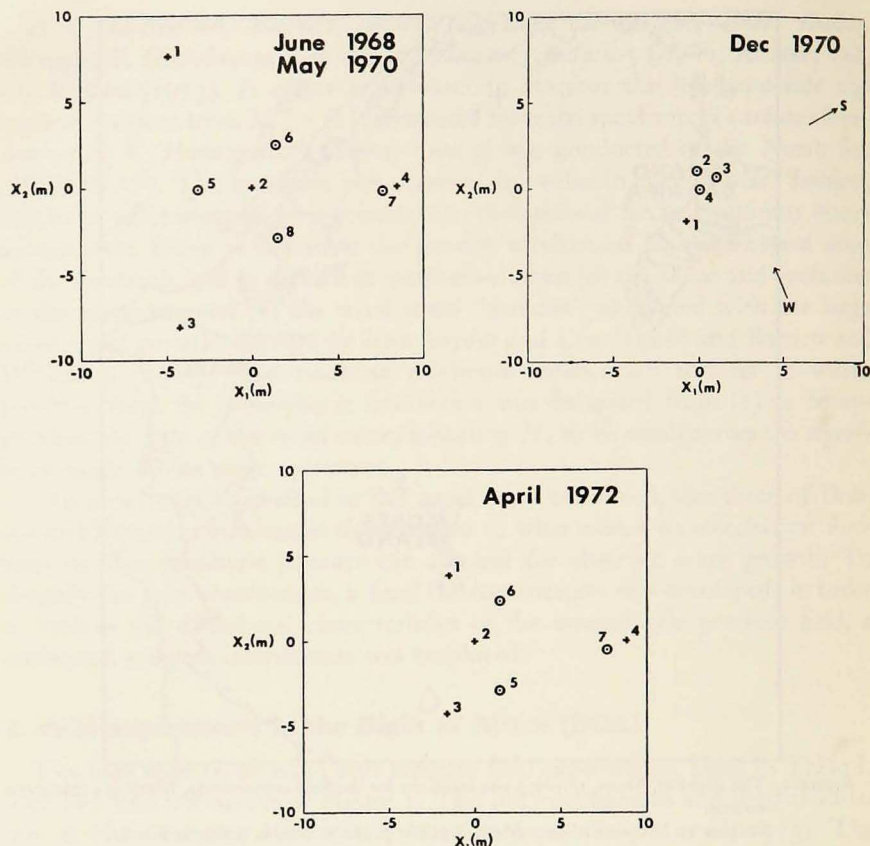
Figure 2. Instrument configurations;

+ — wave recorder

⊙ — microbarograph

Note that during the May 1970 experiment, a cup anemometer was located at wave recorder 2. The December 1970 configurations show the wind direction (*W*) and direction of vessel (*S*) for Run 8.

waves with anomalous dispersion. The particular spacing of instruments did not allow a clear choice between these alternatives. The December 1970 experiment was designed to provide that choice by spacing the instruments a small fraction of the expected wavelength. Following this experiment, it was clear that most of the data collected to that time showed a dominant atmospheric pressure fluctuation traveling upwind with surface gravity wave dispersion (there were several exceptions). The correspondence of the peak frequency in the wave spectra and the atmospheric pressure spectra suggested a local reflection mechanism producing a small upwind-traveling component to the wave spectrum for which the atmospheric pressure fluctuation was greatly amplified

(relative to the downwind component) as a result of the dynamics of the flow. The appearance of an upwind-traveling component in several runs in which the laboratory vessel was not downwind of the array (as it had been during the May 1970 experiment) led to the further conclusion that reflections other than those from the vessel were present, and to the further speculation that such natural reflections might, in fact, dominate. In an effort to examine one possibility, reflection by bottom irregularities, R. B. Long (1973) and this author collaborated in applying the theory of K. Hasselmann (1966) to the data, using an experimentally determined spectrum for the bottom irregularities. The effect proved too small to account for the May 1970 observations. Ultimately, it was decided to recreate, in April 1972, the conditions of the May 1970 experiment in most particulars except for the location of the laboratory vessel (which was placed crosswind from the array). The April 1972 data showed a dominant pressure fluctuation traveling downwind with surface gravity wave dispersion, clearly implicating the laboratory vessel as the principal (but not sole) source of previously observed upwind-traveling waves.

The historical development of the study emphasizes those aspects of the study concerning the nature and directional characteristics of the atmospheric pressure fluctuations. It should be recognized that in terms of the primary objective of the study, determination of the energy and momentum transfer to surface gravity waves, these aspects are somewhat secondary. It will be seen presently that each of the experiments has contributed to a quantitative description of the wave-coherent part of the atmospheric pressure fluctuation, and to an estimate of the resulting energy and momentum transfer to surface gravity waves.

## 3. Preliminary analysis

Preliminary analyses of typical runs from each of the four field experiments are shown in Figures 3–5. Run parameters are given in Table II. Figure 3 shows the raw data for the first 100 s of each run. Figure 4 shows the corresponding raw spectra for the first hour of each run, and Figure 5 shows the raw coherence and phase between selected instrument pairs. Note the similarity between wave-recorder and microbarograph records with respect to characteristic frequency (this similarity is not so striking in Run 5). Note also the characteristic appearance of the atmospheric pressure spectra—a large wave-induced peak superimposed upon a monotonically decreasing background. (These features were also noted by both Dobson (1971) and Elliott (1972).) The peak stands more than an order of magnitude above background in Runs 11, 32, and 8, and somewhat less than an order of magnitude above background in Run 5.

The nature of the atmospheric pressure spectra is clarified by examination of Figure 5. Shown for each run are coherence and phase for selected instrument
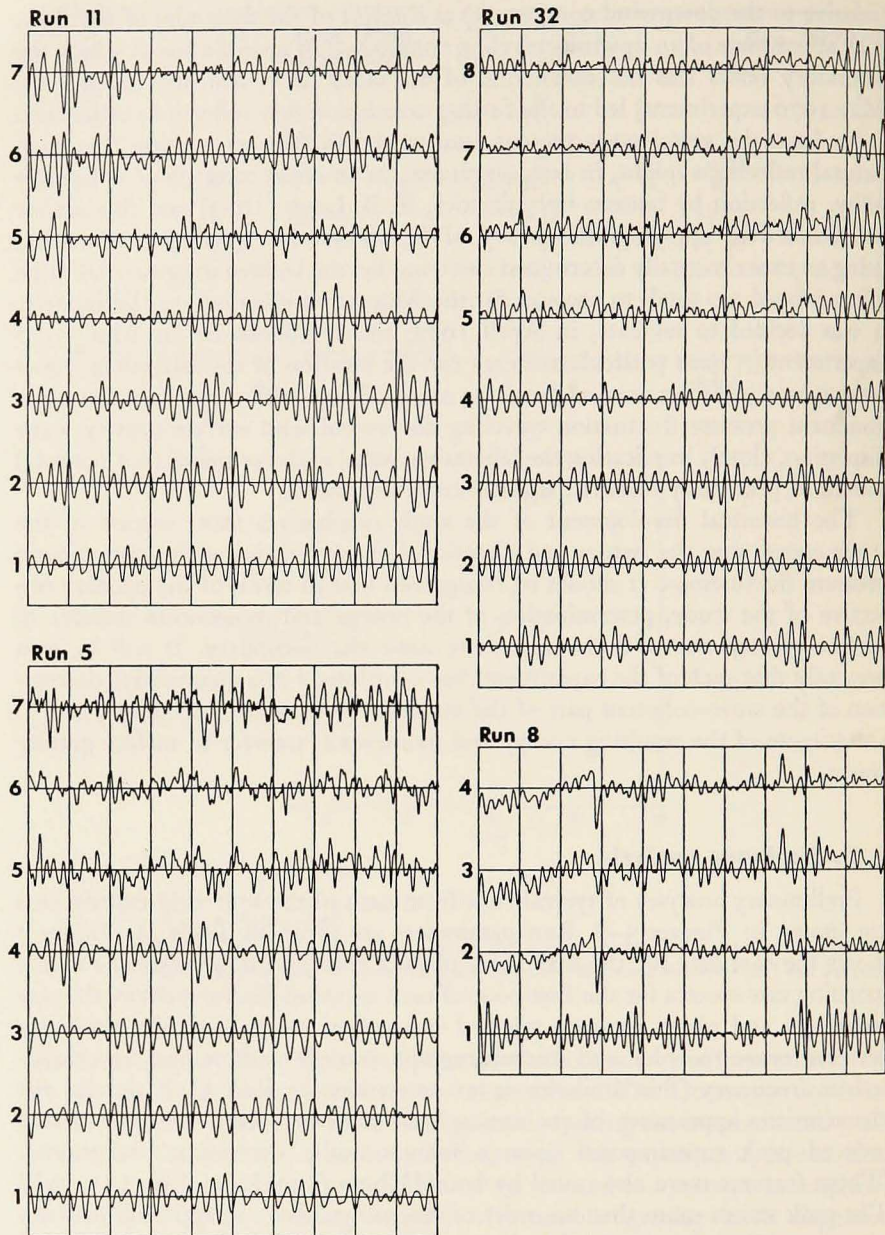
Figure 3. Raw data for Runs 11, 32, 8, and 5.
Instruments numbered as in Figure 2 (see Table II). Instrument 1 (Run 8) and instruments 1–4 (Runs 11, 32, and 5) are wave recorders. The remaining instruments are microbarographs. Horizontal scale is 10 s/div.

Table II. Run parameters.

| Run | Experiment | Wind Speed (m/s) | Wind Direction (°) | Position of Vessel |
|-----|-----------|------------------|---------------------|--------------------|
| 11 | June 1968 | 4.98 | 198 | crosswind |
| 32 | May 1970 | 8.32 | 72 | downwind |
| 8 | December 1970 | 4.80 | 152 | crosswind |
| 5 | April 1972 | 7.89 | 98 | crosswind |

Wind direction is direction of approach in degrees clockwise from N.

pairs. These typically include a microbarograph pair aligned with the wind, a microbarograph pair aligned across the wind, and a closely spaced wave recorder-microbarograph pair. In each case, the phase for the microbarograph pair aligned with the wind rises monotonically from zero at zero frequency, breaks sharply (discontinuity in both phase and slope) at the low-frequency end of the surface gravity wave range, then follows a monotonic trend across this range. In Runs 11, 32, and 8, the slope of this trend is negative, and in Run 5 it is positive. At higher frequencies, the phase becomes less well defined, although in Runs 11 and 5 there appears to be a second break point above which the curve reverts to its original trend. As is seen in the figure, it is possible to account for both major trends in a straightforward manner. The segments labeled T are based on the dispersion relation
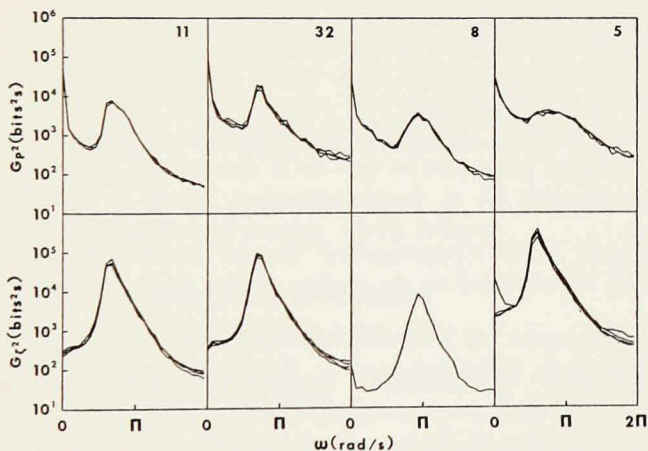


Figure 4. Raw spectra for Runs 11, 32, 8, and 5.
The upper panels show the spectra of atmospheric pressure; the lower panels show the spectra of surface elevation (pressure). All spectra are uncorrected for instrument response and probe elevation. Spectral estimates are Bartlett (1950) estimates with 450 degrees of freedom. The low-frequency rise in the spectrum of surface elevation for Run 8 and for one of the wave recorders in Run 5 is the result of discontinuities in the corresponding records due to the sensitivity of the system to contact resistances in the cable connectors.
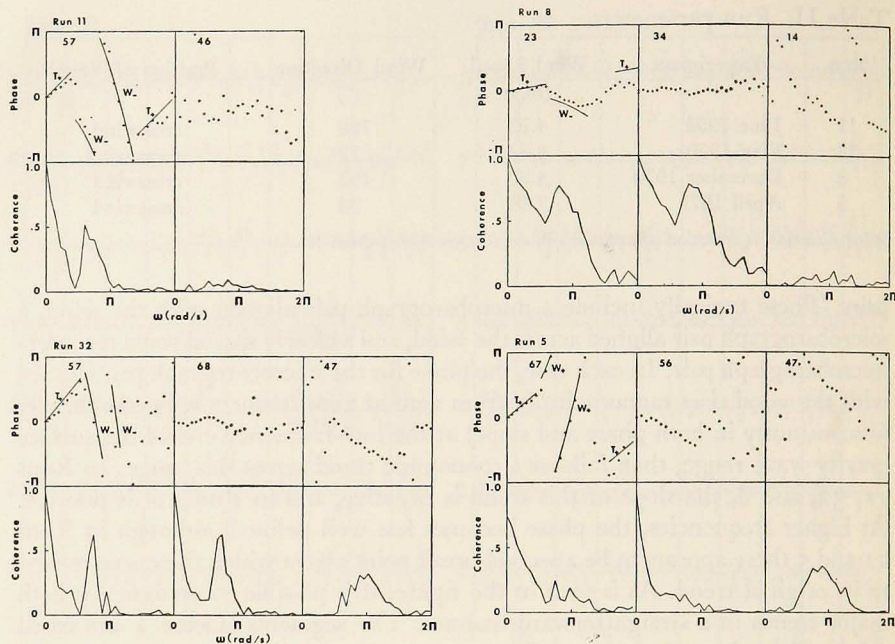
Figure 5. Coherence (lower panel) and Phase (upper panel) for selected instrument pairs, Runs 11, 32, 8, and 5.

For pair identification, see Figure 2 and Table II. Coherence is square coherence. Phase is phase (lead) of the second instrument relative to the first. Curves added to the phase panel of some instrument pairs are theoretical curves based on various dispersions (using wind speed at 5 m).

$T_+$ – frozen turbulence
$W_+$ – downwind-traveling surface gravity waves
$W_-$ – upwind-traveling surface gravity waves

$$\omega(\boldsymbol{k}) = \boldsymbol{k} \cdot \boldsymbol{W},$$

corresponding to Taylor's hypothesis of "frozen" turbulence, while those segments labeled W are based on the surface gravity wave dispersion relation

$$\omega(k) = (gk \tanh kh)^{1/2},$$

where $h$ is the depth. The subscript $+$ denotes a wave traveling downwind, and the subscript $-$ denotes a wave traveling upwind.

Further examination of Figure 5 shows that the phase between microbarographs aligned across the wind hovers about zero over the entire frequency range analyzed, while the coherence between microbarographs aligned both with and across the wind typically begins at a level approaching unity at zero frequency, drops to a minimum at the low-frequency end of the surface gravity wave range, rises to a peak, then drops off at frequencies above the surface gravity wave range.

These observations suggest the following:

1) Over the frequency range analyzed, the atmospheric pressure close to the mean surface appears to be comprised largely of two distinct components, "frozen" turbulence and surface gravity waves.

2) At frequencies above and below the surface gravity wave range, the dominant fluctuation in the atmospheric pressure is associated with "frozen" turbulence.

3) At frequencies within this range, the dominant fluctuation is associated with surface gravity waves. In Runs 11, 32, and 8, this fluctuation is traveling upwind. In Run 5 it is traveling downwind.

4) The level of the atmospheric pressure spectrum in the surface gravity wave range is significantly greater (relative to background) when this spectrum is dominated by upwind-traveling waves than when it is dominated by downwind-traveling waves. Thus,

5) The dominance of upwind-traveling atmospheric pressure waves in the surface gravity wave range in Runs 11, 32, and 8 does not preclude the co-presence of downwind-traveling waves at a level relative to background comparable with Run 5.

The remaining panels in Figure 5 show the coherence and phase between a closely spaced wave recorder-microbarograph pair. Note that the phase is well defined over the surface gravity wave range (since the data has not been corrected for instrument response, no significance should be attached to the particular level or trend of the phase curve), and that the coherence is typically low, rising to broad maxima of .3 and .4 in Runs 32 and 5, staying below .1 in Runs 11 and 8. Not shown are the coherence and phase for more widely separated wave recorder-microbarograph pairs; the corresponding coherence levels here are very low indeed. This lack of coherence (resulting primarily from the presence of several competing signals in the atmospheric pressure) complicates the wave-coherent analysis which follows.

## 4. Averaging and extrapolation procedures

In order to optimize the statistical reliability of the wave-coherent analysis of the atmospheric pressure records, it was decided to adopt the following averaging and extrapolation procedures:

1) All records from the May 1970 experiment, during which the wind blew steadily from slightly north of east, were subdivided into sections of length 469.3 s (1024 data points). The average wind at 5-m elevation and the average microbarograph elevation were computed for each section, and the spectral matrix (referred to as a section matrix) containing the cross-spectral information between all instrument pairs was formed using Bartlett (1950) estimates with 64 degrees of freedom.

Table III. Average spectral matrices, May 1970.

| Microbarograph Elevation (m) | Wind Speed (m/s) | | | | | | | |
|---|---|---|---|---|---|---|---|---|
| | 5.25 | 5.75 | 6.25 | 6.75 | 7.25 | 7.75 | 8.25 | 8.75 |
| .95 ............. | 5 | 4 | 1 | 2 | 3 | 2 | 4 | 1 |
| 1.05 ............. | 1 | 7 | 8 | 3 | 4 | 0 | 5 | 1 |
| 1.15 ............. | 0 | 3 | 3 | 5 | 3 | 0 | 5 | 2 |
| 1.25 ............. | 0 | 3 | 11 | 9 | 11 | 5 | 1 | 2 |
| 1.35 ............. | 0 | 2 | 9 | 9 | 10 | 17 | 17 | 4 |
| 1.45 ............. | 0 | 2 | 8 | 11 | 8 | 11 | 9 | 2 |
| 1.55 ............. | 0 | 2 | 7 | 7 | 9 | 3 | 0 | 0 |
| 1.65 ............. | 0 | 1 | 2 | 1 | 3 | 3 | 2 | 0 |
| TOTAL ............. | 6 | 24 | 49 | 47 | 51 | 41 | 43 | 12 |

2) These section matrices were corrected for instrument response and for the elevation of the wave-recorder probes (wave-recorder related matrix elements were extrapolated to the mean surface in exponential fashion consistent with linear potential theory).

3) Average spectral matrices for like values of wind speed and microbarograph elevation were formed. Table III lists the number of section matrices contributing to the average in each category. The corresponding number of degrees of freedom for the average matrices is obtained by multiplying by 64.

4) The corrected section matrices 2) were "surface normalized" by extrapolating microbarograph related matrix elements to the mean surface in exponential fashion consistent with linear potential theory.

5) An average "surface normalized" spectral matrix was formed for each wind speed from the "surface normalized" section matrices 4). The number of "surface normalized" section matrices contributing to these averages is given in the row labeled TOTAL in Table III.

A somewhat simpler averaging and extrapolation procedure was followed in the case of the April 1972 data:

1) The data were subdivided into sections approximately one hour long. The average wind speed at 5-m elevation and the average microbarograph elevation were computed for each section, and a spectral matrix containing the cross-spectral information between all instrument pairs was formed.

2) These section matrices were corrected for instrument response and for the elevation of the wave-recorder probes, and, using an exponential extrapolation, "surface normalized" for the elevation of the microbarograph probe.

3) The "surface normalized" section matrices were grouped by wind speed, using convenient values for the wind speed. Average spectral matrices

and average wind speeds were calculated for each group. Table IV lists the amount of data contributing to each average spectral matrix and the corresponding mean wind speed.

Support for the exponential extrapolation of microbarograph-related matrix elements is provided in Figure 6,

Table IV. Average spectral matrices, April 1972.

| Wind Speed (m/s) | Hours of Data |
|---|---|
| 6.51 | 1 |
| 7.08 | 3 |
| 7.54 | 3 |
| 7.94 | 1 |
| 8.45 | 6 |
| 9.27 | 2 |

in which the amplitude and phase of the May 1970 cross-spectra between instruments 4 and 7 (a wave recorder-microbarograph pair approximately 1 m apart) are compared at various microbarograph elevations. The amplitude ratio

$$|G_{47}(z)/G_{44}(z)|/|G_{47}(0)/G_{44}(0)|$$

and phase difference

$$\theta(z) - \theta(0) \equiv \arg(G_{47}(z)) - \arg(G_{23}(0))$$

were computed for each frequency band of each average spectral matrix 3). [$G_{47}(z)$ denotes the cross spectrum between instruments 4 (wave recorder) and 7 (microbarograph) obtained for microbarograph elevation $z$, and $G_{44}(z)$ denotes the corresponding autospectrum for instrument 4. (Here $z$ is essentially a label identifying the autospectrum with a corresponding cross-spectrum). The reference spectra, $G_{47}(0)$ and $G_{44}(0)$, are the average "surface normalized" spectra 5) of like wind speed.] These amplitude ratios and phase differences were then averaged across wind speed (the average was weighted by the number of section matrices 1) contributing to each average matrix 3)). The resulting averages are presented in the figure. The scatter in the results of this analysis is attributed to sectional differences in the directional cross-spectrum between surface elevation and atmospheric pressure, associated with the incomplete parameterization of the sea by the local wind.
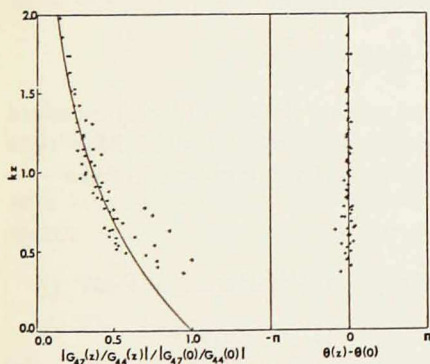
Figure 6 suggests the following conclusions:



Figure 6. Dependence of amplitude and phase of the wave-coherent part of the atmospheric pressure upon elevation above the mean surface.
The solid curves are the predictions of linear potential theory. See text for explanation of figure.

1) The wave-coherent part of the atmospheric pressure decays ex-

ponentially from the mean surface. The decay rate is essentially that predicted by linear potential theory.

2) The phase of the wave-coherent part of the atmospheric pressure is constant with elevation above the mean surface.

While not altogether convincing (The analysis tends, within each frequency band, to place the data points for middle values of $z$ close to the solid curves. That this analysis is not totally self-fulfilling can be seen by applying it to data representing other profiles, for example a constant amplitude with linear change of phase), these conclusions are in substantial agreement with the observations of Elliott (1972) and with various calculations of Long (1971). Elliott finds that close to the surface, the decay parameter is a decreasing function of $k \cdot W/\omega(k)$. According to Long (private communication), the Miles (1957) theory appears to imply a comparable decrease in the decay parameter close to the surface $(kz < 2)$. This decrease is not sufficient to change appreciably the conclusions of the present study. (Elliott's extrapolation would lower the average amplitude of the wave-induced pressure at the surface (as presented in Figure 14) by something like 15%. This lowering would be an increasing function of $k \cdot W/\omega(k)$.) The May 1970 data cannot readily be subjected to the type of analysis employed by Elliott because the cross spectrum $G_{47}$ contains a significant contribution from upwind-traveling waves.

Note that in Figure 6, there is a tendency for the amplitude data to be larger than the potential theory prediction at lower values of $kz$. This tendency may or may not be significant; its sense is opposite to that which would be expected from Elliott's analysis.

Note also that the surface normalization completely distorts the wave-incoherent (turbulent) contribution to the resulting spectral matrices.

## 5. Spectral fits

Figure 7 shows the average spectrum of surface elevation $G_{\zeta^2}(\omega)$ contained in the average "surface normalized" spectral matrices 5) for the May 1970 data. Included in the figure is the Phillips (1958) equilibrium spectrum

$$G_{\zeta^2}(\omega) = \varepsilon g^2 \omega^{-5},$$

with $\varepsilon = 7.3 \times 10^{-3}$. A nonlinear fit to the JONSWAP spectral form

$$H_{\zeta^2}(\varepsilon, \Omega, \gamma, \sigma, \omega) = \varepsilon g^2 \omega^{-5} e^{-\frac{5}{4}\left(\frac{\Omega}{\omega}\right)^4} \gamma e^{-\frac{(\omega-\Omega)^2}{2\sigma^2\Omega^2}} \tag{3}$$

was made for each of these spectra and to the spectra for Dobson's (1971) Runs 3 and 4a and Elliott's (1972) Runs 167/2 and 119/2. The resulting best fit parameters $\varepsilon$, $\Omega$, $\gamma$, and $\sigma$ are given in Table V. Two fits are represented. The first of these minimizes the variance
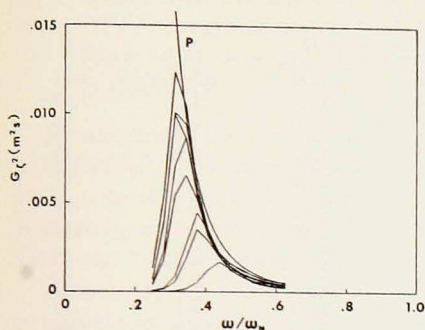
Figure 7. Spectra of surface elevation for the various wind speed categories of the May 1970 data.

$G_{\zeta^2}(\omega)$ is the spectrum of surface elevation. Spectra are shown for wind speeds from 5.25 m/sec to 8.75 m/sec. The Nyquist frequency $\omega_N$ is 6.85 rad/sec. Curve $P$ is the Phillips equilibrium spectrum. Statistical errors are well below the level of systematic differences resulting from the incomplete nature of the wind speed parameterization.
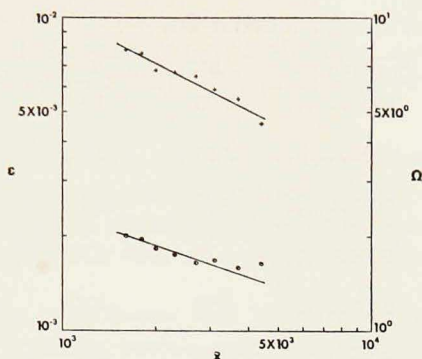
Figure 8. Fetch dependence of spectral fit parameters.

+ — Phillips (1958) parameter, $\varepsilon$
o — nondimensional peak frequency, $\tilde{\Omega}$

$$V = \sum_n (G_{\zeta^2}(\omega_n) - H_{\zeta^2}(\varepsilon, \Omega, \gamma, \sigma, \omega_n))^2 / G_{\zeta^2}(\omega_n)^2 \qquad (4)$$

and tends to give a better fit to the higher frequency tail of the spectrum ($\varepsilon$ more reliable); the second minimizes

$$V = \sum_n (G_{\zeta^2}(\omega_n) - H_{\zeta^2}(\varepsilon, \Omega, \gamma, \sigma, \omega_n))^2$$

and tends to give a better fit to the spectral peak.

On the basis of similar fits, K. Hasselmann *et al* (1973) conclude that for a wide range of observed fetch-limited wave spectra including the JONSWAP spectra and various additional field and laboratory spectra:

1) The spectral form (using a double valued $\sigma$) gives a good fit to the data.
2) The parameters $\varepsilon$, $\tilde{\Omega} \equiv W\Omega/g$, $\gamma$, and $\sigma$ are, allowing some scatter, functions of a single parameter, the nondimensional fetch $\tilde{x} \equiv gx/W^2$. Here $x$ is the fetch and $W$ is the 10 m wind speed.
3) $\varepsilon$ is an inverse function of $\tilde{x}$ and is approximated by the power law $\varepsilon \simeq .076$ $\tilde{x}^{-.22}$, over the range $\tilde{x} = 10^{-1}$ to $10^5$. In the limited range $\tilde{x} = 10^2$ to $10^4$, however, a somewhat larger exponent ($\sim -.4$) is more appropriate to the data.

Table V. Spectral fits.

| Spectrum | $W$ | $\tilde{x}$ | $\varepsilon$ | $\Omega$ | $\gamma$ | $\sigma$ |
|---|---|---|---|---|---|---|
| 2001...... | 5.25 | 4.4 | 4.6 | 3.06 | 3.6 | .11 |
|  |  |  | 4.4 | 3.04 | 3.5 | .13 |
| 2002...... | 5.75 | 3.7 | 5.5 | 2.71 | 3.3 | .12 |
|  |  |  | 5.8 | 2.67 | 2.9 | .11 |
| 2003...... | 6.25 | 3.1 | 5.9 | 2.64 | 3.6 | .11 |
|  |  |  | 6.1 | 2.61 | 3.3 | .11 |
| 2004...... | 6.75 | 2.7 | 6.4 | 2.40 | 3.0 | .14 |
|  |  |  | 6.5 | 2.36 | 2.8 | .15 |
| 2005...... | 7.25 | 2.3 | 6.7 | 2.37 | 3.5 | .13 |
|  |  |  | 7.0 | 2.33 | 3.1 | .12 |
| 2006...... | 7.75 | 2.0 | 6.8 | 2.32 | 3.4 | .14 |
|  |  |  | 7.4 | 2.25 | 2.9 | .12 |
| 2007...... | 8.25 | 1.8 | 7.7 | 2.33 | 3.3 | .13 |
|  |  |  | 7.7 | 2.26 | 3.0 | .13 |
| 2008...... | 8.75 | 1.6 | 7.9 | 2.26 | 3.4 | .13 |
|  |  |  | 8.3 | 2.23 | 3.1 | .11 |
| Dob 3 .... | 3.4 | 5.6 | – | – | – | – |
|  |  |  | 23.9 | 3.18 | .13 | .16 |
| Dob 4a ... | 8.0 | .4 | 6.0 | 2.59 | .38 | .13 |
|  |  |  | 10.5 | 3.10 | .68 | .03 |
| E11 167/2 ... | 7.9 | 1.0 | 5.3 | 3.13 | 5.2 | .14 |
|  |  |  | 3.5 | 3.13 | 7.3 | .18 |
| E11 119/2 ... | 4.7 | 1.1 | 3.1 | 3.40 | 2.0 | .10 |
|  |  |  | 2.8 | 3.40 | 2.0 | .14 |

$W$ – wind speed in m/s
$\tilde{x}$ – nondimensional fetch in units of $10^3$
$\varepsilon$ – Phillips (1958) parameter in units of $10^{-3}$
$\Omega$ – peak frequency parameter in rad/s
$\gamma$ – peak enhancement factor
$\sigma$ – peak shape parameter

4) $\tilde{\Omega}$ is an inverse function of $\tilde{x}$ and is well approximated by the power law, $\tilde{\Omega} \simeq 22. \ \tilde{x}^{-.33}$, over the entire range $\tilde{x} = 10^{-1}$ to $10^5$.

5) $\gamma$ and $\sigma$ are essentially constant, with $\gamma \simeq 3.3$ and $\sigma \simeq .07, .09$ over the range $\tilde{x} = 10^2$ to $10^4$.

Inspection of Table V for the May 1970 data (spectral fit (4)) indicates that for this data, the parameters $\gamma$ and $\sigma$ are independent of $\tilde{x}$ and have values comparable to the JONSWAP values, with $\gamma \simeq 3.4$ and $\sigma \simeq .12$. Figure 8 shows the corresponding dependence of $\varepsilon$ and $\tilde{\Omega}$ on $\tilde{x}$ for the May 1970 data. $\varepsilon$ and $\tilde{\Omega}$ are well approximated by the power laws (not best fits), $\varepsilon = .32 \ \tilde{x}^{-1/2}$ and $\tilde{\Omega} = 23.5 \ \tilde{x}^{-1/3}$. Comparison with JONSWAP indicates the following:

1) The power law for $\tilde{\Omega}$ is comparable with the JONSWAP result.

2) $\varepsilon$ is smaller than for JONSWAP. The exponent of $-1/2$ is, however, con-

sistent with the trend of the JONSWAP data in the range $\tilde{x} = 10^2$ to $10^4$. A rough fit to the JONSWAP data gives $\varepsilon \simeq .57\,\tilde{x}^{-1/2}$. Thus the May 1970 data are characterized by an $\varepsilon$ roughly $^1/_2$ as large as for JONSWAP.

In summary, the spectral fits for the May 1970 data are consistent with JONSWAP in every respect save one: the spectra are half as large. The difference in the fetch distribution (with angle) is probably responsible for this reduction; what is surprising is that this difference does not appear to seriously affect the "shape" of the spectrum.

Because of the consistency of the May 1970 spectra with JONSWAP, it is possible to apply JONSWAP results (ignoring possible complications from the skewed directional distribution) directly to these spectra. In particular, one can estimate the nonlinear transfer from calculations made for the mean JONSWAP spectrum. Because the transfer scales as $\varepsilon^3$, one would expect it to be approximately one-sixth as large as for JONSWAP.

The spectral fits to Dobson's (1971) and Elliott's (1972) runs, obtained on the Spanish Bank, do not support in any consistent fashion the scaling conclusions of JONSWAP. The fits to the spectral form (3) are not as stable as those for the May 1970 data (due perhaps in part to the difficulty in accurately transcribing values from the published figures) and resulting best fit parameters, with the exception of $\sigma$, differ considerably from JONSWAP. Nonetheless, several conclusions may be drawn from the fits:

1) The Spanish Bank spectra, like the May 1970 spectra, are typically less "well developed" than the JONSWAP spectra. (Dobson's Run 3 has $\varepsilon \sim 20$. Note however that $\varepsilon\gamma \sim 3$ as compared with $\varepsilon\gamma \sim 15$ for spectrum 2001.) Thus,

2) The nonlinear transfer associated with these spectra should also be "relatively" small.

## 6. Directional spectrum and directional cross-spectrum analysis

It can be shown (e.g., Snyder, 1973) that for a linear sea, the covariances

$$C_{\zeta^2} \equiv \,< \zeta(x,t)\,\zeta(x+\xi,t+\tau) >,$$
$$C_{\zeta P} \equiv \,< \zeta(x,t)\,P(x+\xi,t+\tau) >,$$
and
$$C_{P^2} \equiv \,< P(x,t)\,P(x+\xi,t+\tau) >,$$

where $P$ is the wave-coherent atmospheric pressure at the mean surface and the brackets denote an ensemble average, are expressible in terms of the spectra

$$C_{\zeta^2} = \int d^2k F_{\zeta^2}(k)\cos\,(k\cdot\xi - \omega(k)\tau),$$
$$C_{\zeta P} = \mathrm{Re}\,\{\int d^2k F_{\zeta P}(k)\,e^{i\,(k\cdot x - \omega(k)\tau)}\},$$

and
$$C_{P^2} = \int d^2k F_{P^2}(\boldsymbol{k}) \cos{(\boldsymbol{k} \cdot \boldsymbol{\xi} - \omega(k)\tau)}.$$

The related spectra

$$E_{\zeta^2}(\omega,\theta) \equiv \frac{\omega^3}{g^2} F_{\zeta^2}(\boldsymbol{k}(\omega,\theta)),$$

$$E_P^2(\omega,\theta) \equiv \frac{\omega^3}{g^2} F_{P^2}(\boldsymbol{k}(\omega,\theta)),$$

and

$$E_{\zeta P}(\omega,\theta) \equiv \frac{\omega^3}{g} F_{\zeta P}(\boldsymbol{k}(\omega,\theta)),$$

will be referred to as the directional spectra for $\zeta$ and $P$ and the directional cross-spectrum between $\zeta$ and $P$, respectively.

Estimates of the directional spectra for $\zeta$ were obtained from the spectral matrices by assuming an expansion of the form

$$E_{\zeta^2}(\omega,\theta) = \sum_{n=1}^{N} {}_nE_{\zeta^2}(\omega)\,\psi_n(\theta-\theta_W), \qquad \text{linear analysis,}$$

or

$$E_{\zeta^2}(\omega,\theta) = \left(\sum_{n=1}^{N} {}_nE_{\zeta^2}(\omega)\,\psi_n(\theta-\theta_W)\right)^2, \qquad \text{bilinear analysis,}$$

with ${}_nE_{\zeta^2}(\omega)$ real. $\theta_W$ is the wind azimuth. Similar analyses were made for $E_{P^2}(\omega,\theta)$. Estimates of the directional cross-spectrum were obtained by assuming an expansion of the form

$$E_{\zeta P}(\omega,\theta) = \sum_{n=1}^{N} {}_nE_{\zeta P}(\omega)\,\psi_n(\theta-\theta_W),$$

with ${}_nE_{\zeta P}(\omega)$ complex.

Several choices of a basis set were employed:

Type 1:　$\psi_n(\theta) \equiv \cos{(n-1)\theta/2}, \ n$ odd,
$\equiv \sin{n\theta/2}, \ n$ even.

In the linear case, this choice reduces to the Fourier-Bessel analysis described by Gilchrist (1966).

Type 2:　$\psi_n(\theta) \equiv \cos^m\theta \cos{(n-1)\theta/2}, \ n$ odd,
$\equiv \cos^m\theta \sin{n\theta/2}, \ n$ even.

$m$ is typically 2 or 4. This choice tends to emphasize the downwind and upwind lobes of the spectrum.

Type 3:　$\psi_n(\theta) \equiv \cos^m\theta \cos{(n-1)\theta}, \cos\theta > 0, \ n$ odd,
$\equiv \cos^m\theta \sin{n\theta}, \cos\theta > 0, \ n$ even,
$\equiv 0, \cos\theta < 0.$

This choice does not allow wave components traveling against the wind.

The linear analysis involves a linear least-squares fit to sub-matrices contained in the spectral matrix. The bilinear analysis involves a bilinear least-squares fit to these submatrices. This fit is accomplished by choosing some initial set

$$_nE_{\zeta^2}^{(0)}(\omega), n = 1, 2, \ldots, N$$

and solving iteratively the linear least-squares problem arising from the representation

$$E_{\zeta^2}(\omega, \theta) = \sum_{\substack{n=1 \\ m=1}}^{\substack{M \\ N}} {}_nE_{\zeta^2}^{(i-1)}(\omega) \, {}_mE_{\zeta^2}^{(i)}(\omega) \, \psi_n(\theta - \theta_W) \, \psi_m(\theta - \theta_W), i = 1, 2, \ldots$$

Convergence is typically achieved by replacing the resulting $_mE_{\zeta^2}^{(i)}(\omega)$ by

$$\frac{1}{2} \{ {}_mE_{\zeta^2}^{(i)}(\omega) + {}_mE_{\zeta^2}^{(i-1)}(\omega) \}.$$

Considerable difficulty typically was encountered at higher frequencies in producing an acceptable fit to the appropriate submatrix. This difficulty was in part the result of the low coherence between wave records at these frequencies resulting from the too-wide spacing of instruments. Some improvement in the fit typically resulted by allowing for a small drift current ($<.2$ m/sec). Because the currents at Site 1 (tidal and wind-driven) are small, the necessity for a drift correction has fairly general implications regarding the study of higher-frequency gravity waves at any field site. Dobson (private communication) also points out that the presence of this drift may systematically bias the spectral fit parameters (in particular, $\varepsilon$) of Section 5.

Figures 9 and 10 show the directional spectra for surface elevation $E_{\zeta^2}$ and directional cross-spectrum between surface elevation and atmospheric pressure $E_{\zeta P} = P_{\zeta P} + iQ_{\zeta P}$ estimated from the average spectral matrices for the May 1970 and the April 1972 data.

The following features should be noted:

1) In both cases, $E_{\zeta^2}$ is significant only within about $\pm 45°$ of the wind azimuth. In the case of the April 1972 data, $E_{\zeta P}$ also is significant only within about $\pm 45°$ of the wind azimuth.
2) In the May 1970 data, $E_{\zeta P}$ has a primary lobe centered downwind and a secondary lobe centered upwind.
3) The location of the maximum in the directional distribution for both $E_{\zeta^2}$ and $E_{\zeta P}$ is frequency-dependent. This dependence is consistent with the geometry of the Site 1 region. It is less marked for $E_{\zeta P}$ than for $E_{\zeta^2}$.
4) $P_{\zeta P}$ is typically negative, $Q_{\zeta P}$ typically positive.
5) The angular distribution for $Q_{\zeta P}$ is typically bimodal for frequencies above the peak frequency.
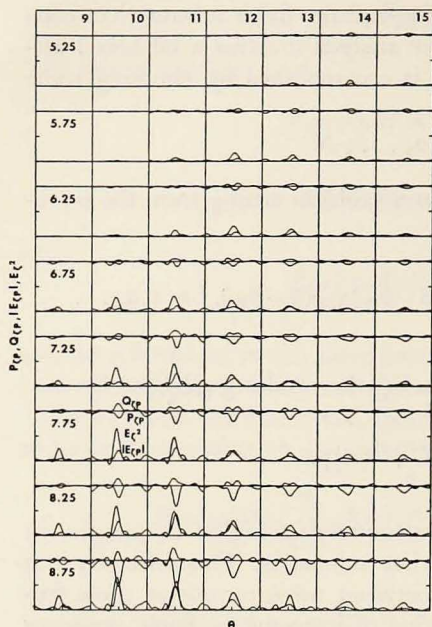
Figure 9. Directional spectra and directional cross-spectra for the May 1970 average spectral matrices.
Scale for $P_{\zeta P}$, $Q_{\zeta P}$, and $|E_{\zeta P}|$ is .04 Ns/m (Newton second/meter) per division. Scale for $E_{\zeta^2}$ is .01 m²s per division. Scale for $\theta$ is $\pi$ per division. Directional distributions are centered on West (travel towards). The frequency band is noted across the top of the panel, the wind speed (m/s) down the left side. (The mean wind azimuth was approximately 080°). The Nyquist band was 32 and the Nyquist frequency 6.85 rad/sec. Estimates for $E_{\zeta P}$ were linear estimates of Type 2 (modified), with $N = 9$, m = 2. Estimates for $E_{\zeta^2}$ were linear estimates of Type 3, with $N = 5$, m = 2.
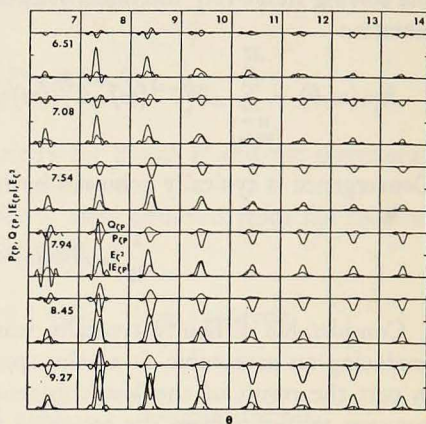
Figure 10. Directional spectra and directional cross-spectra for the April 1972 average spectral matrices.
Scale for $P_{\zeta P}$, $Q_{\zeta P}$, and $|E_{\zeta P}|$ is .04 Ns/m per division. Scale for $E_{\zeta^2}$ is .01 m²s per division. Scale for $\theta$ is $\pi$ per division. Directional distributions are centered on West (travel towards). The frequency band is noted across the top of the panel and the wind speed (m/s) down the left side. (The mean wind azimuth was approximately 100°.) The Nyquist band was 32 and the Nyquist frequency 7.54 rad/sec. Estimates for both $E_{\zeta P}$ and $E_{\zeta^2}$ were linear estimates of Type 3, with $N = 5$, m = 2.
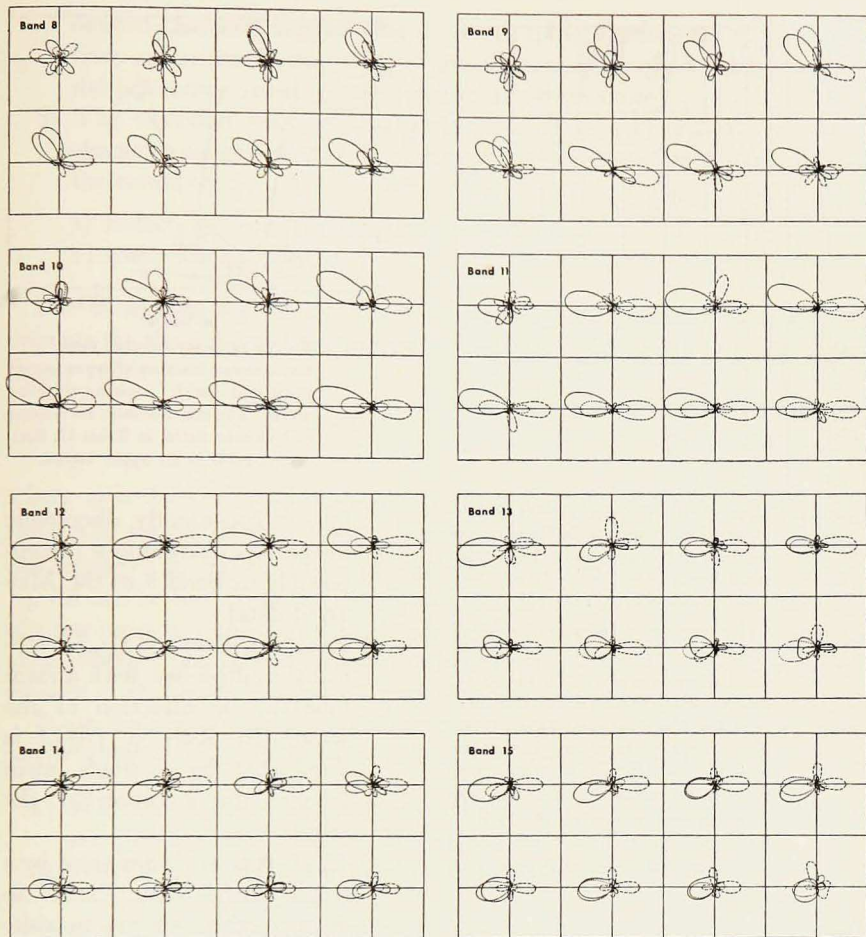
## 7. Upwind-traveling waves

Figures 11 and 12 show normalized polar plots for $E_{\zeta^2}$, $|E_{\zeta P}|$, and $E_{P^2}$ for the May 1970 data, for Runs 10 and 11 from June 1968, and for Run 5 from April 1972. In the latter three cases, the vessel was cross-wind from the array—to the WNW in Runs 10 and 11, and to the S in Run 5.

The following features are noted:

Figure 11. Normalized directional spectra and directional cross-spectra for the May 1970 data, bands 8–15.

$$\text{————————} - E_{\zeta^2}$$
$$\text{— — — — — —} - |E_{\zeta P}|$$
$$\text{— — — — —} - E_{P^2}$$

Spectra are normalized within each band with respect to their integral over $\theta$. Subpanels show spectra within each frequency band for the eight categories of wind speed in the May 1970 analysis. Wind speed increases from left to right, top to bottom of the subpanel. The Nyquist band was 32, the Nyquist frequency 6.85 rad/sec. Estimates for $E_{\zeta^2}$ and $E_{P^2}$ were bilinear estimates of Type 1, with $N = 7$. Estimates for $E_{\zeta P}$ were linear estimates of Type 1, with $N = 9$.

1) $E_{\zeta^2}$ is typically dominated by a single main lobe in the direction of the wind. The axis of the lobe shifts somewhat with frequency in a manner consistent with the geometry of the Bight region. No significant upwind
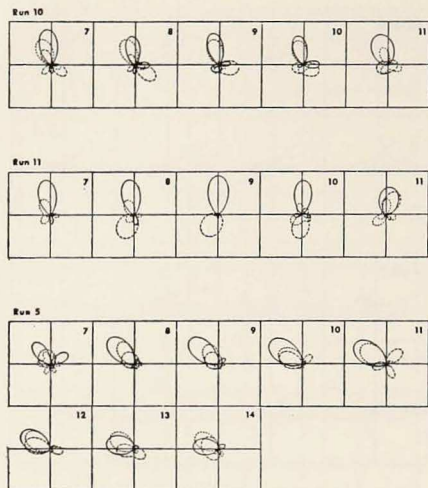
Figure 12. Normalized directional spectra and directional cross-spectra for Runs 10 and 11 from July 1968, and Run 5 from April 1972.

$$\text{————} - E_{\zeta 2}$$
$$\text{- - - - - - -} - |E_{\zeta P}|$$
$$\text{— — — — —} - E_{P2}$$

Normalization is similar to Figure 11. Subpanels show spectra for the three runs for the frequency bands listed. The Nyquist band in each case was 32, the Nyquist frequency 7.54 rad/sec. Estimates for $E_{\zeta 2}$ and $E_{P2}$ were bilinear estimates of Type 1, with $N = 5$. Estimates for $|E_{\zeta P}|$ were linear estimates of Type 1, with $N = 7$.
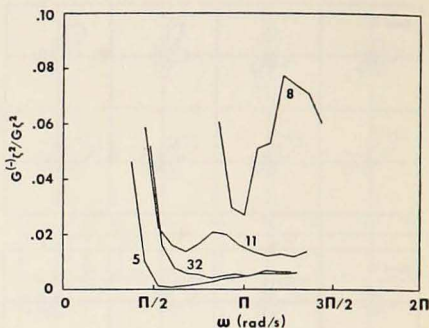


Figure 13. Energy ratio for selected runs. Ratio shows fraction of wave energy associated with upwind-traveling waves. The run numbers correspond to the runs listed in Table II. Estimated ratio is an upper bound.

lobe is consistently discernible in the $E_{\zeta 2}$ distributions (except possibly in Band 8 of the May 1970 data).

2) Except in Run 5, $|E_{\zeta P}|$ is typically multi-lobed with a main lobe in the direction of the wind. In Run 5, $|E_{\zeta P}|$ is dominated by a single main lobe in the direction of the wind.

3) $E_{P2}$ is typically dominated by a single main lobe. Except in Run 5, this lobe is opposite the direction of the wind. In Run 5, this lobe is in the direction of the wind.

4) The presence of a significant downwind lobe for $|E_{\zeta P}|$ in all cases implies the presence of downwind-traveling, wave-coherent atmospheric pressure fluctuations in all cases.

5) The direction associated with the main lobe of $E_{P2}$ implies that except in Run 5, the downwind-traveling atmospheric pressure fluctuations are dominated by upwind-traveling atmospheric pressure fluctuations.

6) The direction associated with the upwind lobes of $|E_{\zeta P}|$ and $E_{P2}$ and its frequency independence suggest that in the May 1970 experiment, the upwind-traveling fluctuations are primarily the result of reflections from the laboratory vessel.

7) The direction associated with the upwind lobe of $E_{P2}$ and its well-

defined character suggest that in Run 11 the upwind-traveling fluctuations are primarily the result of some source other than reflections from the laboratory vessel (possibly reflections from shore).

8) The direction associated with the upwind lobe of $E_{P2}$ and its broad character suggest that in Run 10 the upwind-traveling fluctuations are the result of:

   a) reflections from the laboratory vessel, and
   b) some other source.

For those runs for which $E_{P2}$ is dominated by an upwind lobe, a rough estimate for the upwind-traveling contribution to $G_{\zeta^2}$ is given by the potential theory result

$$G_{\zeta^2}^{(-)}(\omega) = \left(\frac{1}{s\varrho g}\right)^2 \left(\frac{\omega}{kW + \omega}\right)^4 G_{P^2}(\omega),$$

where $s\varrho$ is the density of air and $g$ is the acceleration of gravity. Using this result and taking $W$ as the wind speed at 5-m elevation, the ratio $G_{\zeta^2}^{(-)}/G_{\zeta^2}$ was estimated for the four runs of Table II. These ratios are shown in Figure 13. As can be seen from the figure, the spectral ratio is typically of the order of a few percent, implying an amplitude ratio of the order of 10%. It is perhaps moot whether one should be able to discern the upwind-traveling component visually at this level. Suffice it to say that the author was not able to do so.

In attempting to understand the presence of upwind-traveling surface gravity waves in the atmospheric pressure fluctuation, one must answer two questions:

1) Why are these waves sometimes dominant in the atmospheric pressure, yet undiscernible in the surface elevation?
2) What is (are) the source(s) of these waves?

An answer to the first question is provided by the dynamics of the flow which imply that the atmospheric pressure is of order

$$P \sim \frac{\varrho}{k}(\boldsymbol{k} \cdot \boldsymbol{W} - \omega)^2 \zeta.$$

It follows that

$$\frac{G_{P^2}^{(-)}}{G_{P^2}^{(+)}} \sim \frac{(kW + \omega)^4}{(kW - \omega)^4} \frac{G_{\zeta^2}^{(-)}}{G_{\zeta^2}^{(+)}}.$$

For $kW \sim \omega$ it is clear that the ratio between the atmospheric pressure spectra should be very much greater than the ratio between the spectra of surface elevation.

A partial answer to the second question has already been suggested. Among the possible sources are:

1) Reflection (scattering) from the laboratory vessel. During the May 1970 experiments this vessel, the L. F. R. Bellows, was located approximately 125 m downwind from the array. The 22 m vessel (6 m beam) was moored bow on, but she typically moved about her mooring so as to present first one bow to the wind, then the other. While it is difficult to estimate precisely how effective a reflector (scatterer) such a vessel would be, one would expect the ratio between the reflected (scattered) and incident energy to be of order $r/D$, where $r$ is the effective radius of the reflector (scatterer) and $D$ the distance to the point of observation. Taking $r$ as 3 m and $D$ as 125 m gives a ratio of $\sim .02$, in good agreement with Figure 13.

2) Reflection (scattering) from the microbarograph housings. This possibility is ruled out as a major source by the low coherence between the wave recorder and microbarograph signals.

3) Reflections from shore. It appears that such reflections could account for some, but not all, of the data obtained when the laboratory vessel was crosswind from the array (i.e., Run 11 of June 1968, but not Run 8 of December 1970).

4) Bottom scattering. The scattering of surface gravity waves by bottom irregularities was first treated by K. Hasselmann (1966). Hasselmann's theory has recently been reinvestigated by Long (1973). Long and this author attempted to evaluate this mechanism at Site 1, using an experimentally determined spectrum for the bottom irregularities (a pressure transducer was dragged across the bottom). The effect was found to be too small, by several orders of magnitude, to account for the May 1970 data.

5) Nonlinear interactions. While it is clear that a spectrum which is initially confined to a downwind half-space cannot, through nonlinear interactions, give rise to components in the opposing upwind half-space (this would violate energy and momentum conservation), it seems possible that the presence of even a single upwind component could, through nonlinear interactions, lead to an entire spectrum of upwind-traveling components. Such a mechanism would feed upon the decay of one or more upwind-traveling components. The decay of such a component was the subject of a study by K. Hasselmann (1963), but the effect on the local spectrum was not investigated.

## 8. Wave-coherent analysis

The rates at which energy and momentum are transferred into the wave field as a result of normal forces acting on unit area of water surface are, to second order
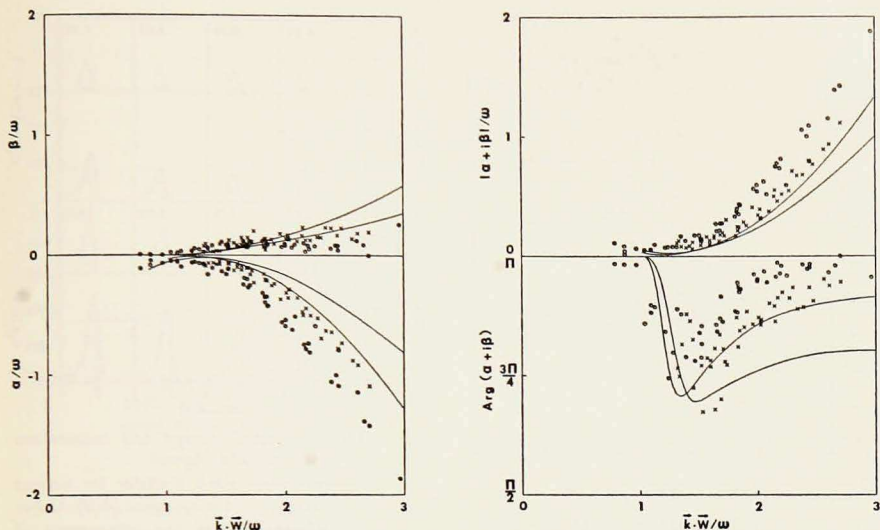
$$\varphi = <P\frac{\partial \zeta}{\partial t}>$$

8

Figure 14. Comparison with Miles (1957) theory.

$$\alpha \equiv \frac{\omega P_{\zeta P}}{\varrho g E_{\zeta^2}},$$

$$\beta \equiv \frac{\omega Q_{\zeta P}}{\varrho g E_{\zeta^2}}.$$

$W$ is the wind speed at 5 m. Curves are included from Miles' theory for $\Omega = 2 \times 10^{-2}$, $3 \times 10^{-3}$. In each subpanel, the curve for $\Omega = 3 \times 10^{-3}$ is the curve giving the better fit to the data.

×  – May 1970 data
o  – April 1972 data

and
$$\tau = <P\nabla\zeta>,$$

respectively, where the pressure field is evaluated at the mean surface.

It can be further shown, using the formalism of Section 6, that

$$\varphi = Re\left\{\int d^2k\,\omega F_{\zeta P}\right\} = \int_0^\infty d\omega \int_0^{2\pi} d\theta\,\omega Q_{\zeta P}$$

and

$$\tau = Re\left\{\int d^2k\,\mathbf{k}F_{\zeta P}\right\} = \int_0^\infty d\omega \int_0^{2\pi} d\theta\,\mathbf{k}Q_{\zeta P}.$$

The integrands $\omega Q_{\zeta P}$ and $\mathbf{k}Q_{\zeta P}$ may be interpreted as the differential rate of energy and momentum transfer to a given wave component. Comparison with eq. (1) yields the following estimate for the growth rate parameter $\beta$:
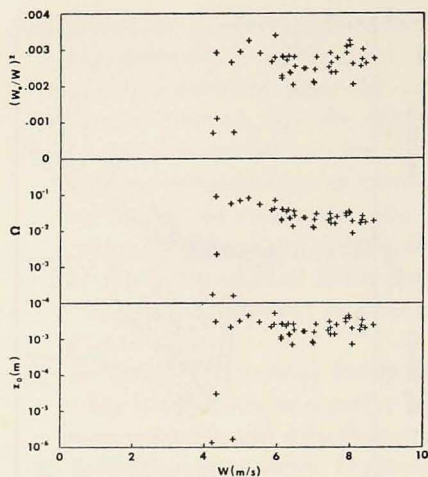
Figure 15. Wind data, May 1970.

$W$ – wind at 5-m elevation
$W_*$ – friction velocity
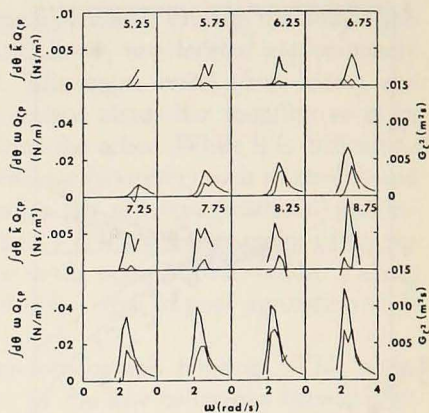$\Omega$ – wind profile parameter
$z_0$ – roughness length

Figure 16. Differential energy and momentum transfer, May 1970.

Subpanels show transfer for various categories of wind speed (m/s). Upper subpanels show the components of the differential momentum transfer in the direction of the wind and at right angles to the wind. (The transfer in the direction of the wind is larger.) Lower subpanels show the differential energy transfer and the wave spectrum (the wave spectrum is defined over the larger frequency range).

$$\beta = \frac{\omega Q_{\zeta P}}{\varrho g E_{\zeta^2}}.$$

Figure 14 shows the estimates for $\alpha \equiv \omega P_{\zeta P}/\varrho g E_{\zeta^2}$ (not to be confused with the parameter $\alpha$ appearing in eq. (1)), $\beta$, $|\alpha + i\beta|$, and $\arg(\alpha + i\beta)$, obtained from the average spectral matrices and associated directional spectra and directional cross-spectra for the May 1970 and the April 1972 data. These parameters are nondimensionalized and are plotted as functions of the parameter $k \cdot W/\omega$. Curves corresponding to Miles' (1957) theory are included for two values of the profile parameter (not to be confused with the spectral fit parameter $\Omega$)

$$\Omega \equiv \frac{g z_0 \varkappa^2}{W_*^2},$$

where $g$ is the acceleration of gravity, $z_0$ is the roughness length, $\varkappa$ is Von Karman's constant, and $W_*$ is the friction velocity. The data points in the figure were obtained by averaging $E_{\zeta^2}$ and $Q_{\zeta P}$ over a range of $\theta$ centered on the peak of $E_{\zeta^2}$. Points are included for each frequency band of each average spectral matrix.

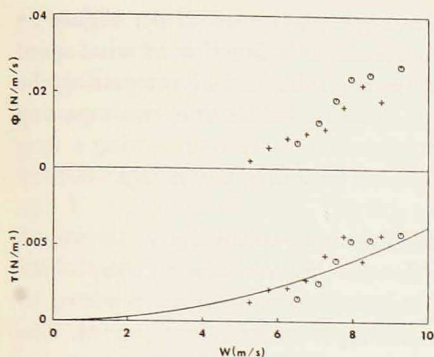An analysis of the wind data obtained in the May 1970 experiment is shown

Figure 17. Energy and momentum transfer, May
1970 and April 1972. $W$ is wind
speed at 5-m elevation.

+ – May 1970
o – April 1972

Curve shown is 2% of the wind
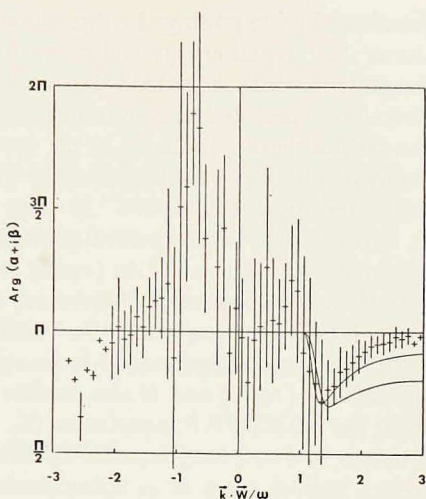stress for a drag coefficient of
.0026.



Figure 18. Phase of atmospheric pressure rela-
tive to surface elevation. Parameters
are defined in Figure 17. Error bars
are explained in the text.

in Figure 15. This analysis is based on a least-squares fit of hourly averages for
two cup anemometers (nominally 5 m and 1.5 m above the water surface) to
the log profile

$$W = \frac{W_*}{\varkappa} \, ln\,(z/z_0).$$

Resulting values for the 5-m drag coefficient $(W_*/W)^2$, the roughness length
$z_0$, and the profile parameter $\Omega$ are shown in the figure. The drag coefficient,
though somewhat large, is comparable with other profile measurements taken
at sea (see Fig. 2.1 of K. Hasselmann *et al*, 1973). The profile parameter $\Omega$
is comparable with the larger of the Miles values included in Figure 14.

Qualitatively, the experimental data of Figure 17 are comparable with the
predictions of the Miles theory. However:

1) These data suggest a smaller effective profile parameter than that esti-
mated from the wind data.

2) The observed pressure signal appears to be somewhat larger than the
Miles prediction. Note that Elliott's (1972) extrapolation would reduce
this discrepancy.

3) There appears to be a systematic difference between the May 1970 and
the April 1972 data.

Figure 16 shows the differential energy and momentum transfer as a func-
tion of frequency for the eight wind-speed categories of the May 1970 data

(obtained by integrating the directional cross-spectrum over all $\theta$); Figure 17 shows the integral energy and momentum transfer as a function of wind speed for both the May 1970 and the April 1972 data (obtained by integrating the directional cross-spectrum over all $\theta$ and over a limited range of $\omega$ encompassing the spectral peak). Included in the latter figure is a curve representing a drag coefficient of $.05 \times 10^{-3}$ or 2% of the wind stress for a drag coefficient of .0026 (the 1970 average).

It is clear that the observed pressure field cannot explain the wave growth observed by Snyder and Cox (1966) and Barnett and Wilkerson (1967). The growth rate parameter $\beta$ is an order of magnitude smaller than reported by Dobson (1971) and a factor of 2 smaller than reported by Elliott (1972). The estimated momentum transfer is an order of magnitude smaller than reported by Dobson (1971) and is also smaller than the minimum transfer estimated from the JONSWAP experiment (K. Hasselmann *et al*, 1972). (The present estimate is biased low, because the associated integration was performed only over a limited range of $\omega$ encompassing the spectral peak. A more complete integration would probably increase the transfer by as much as a factor of 2). It will be seen in the following section that the apparent discrepancy between the present results and JONSWAP is easily resolved. The discrepancy between these results and those of Dobson is not.

The presence of upwind-traveling surface gravity waves discernible in the directional cross-spectrum between atmospheric pressure and surface elevation allows a determination of the energy and momentum transfer associated with these waves. (Because the upwind-traveling waves are not discernible in the directional spectrum of surface elevation, however, the corresponding growth (decay) rates cannot be determined directly.) Figure 18 shows the phase angle between atmospheric pressure and surface elevation for all data from May 1970 and April 1972 averaged within each category of $\boldsymbol{k} \cdot \boldsymbol{W}/\omega$. The phase angles were determined by building a statistical population for $P_{\zeta P}$ and $Q_{\zeta P}$ within each category. Contributions to these populations were accepted for $|E_{\zeta P}| > .15 \, |E_{\zeta P}|_{\max}$, where $|E_{\zeta P}|_{\max}$ is the largest value for $|E_{\zeta P}|$ (defined for 40 values of $\theta$) within a given frequency band. The average phase and r.m.s. phase deviation shown in the figure were computed from the corresponding average and mean square values for $P_{\zeta P}$ and $Q_{\zeta P}$. The figure clearly suggests that waves traveling faster than the wind or against the wind are damped. Note, however, that for $\boldsymbol{k} \cdot \boldsymbol{W}/\omega < -2$ there is some indication that the corresponding waves may grow.

## 9. Implications regarding the energy and momentum balance

The considerations of Sections 5 and 8 suggest that in discussing various experimental results on the wind generation of waves in fetch-limited regions, it is important to distinguish between two different situations:

1) The wind is perpendicular to a long straight coast. The resulting sea will be termed "normally developed".

2) The wind is not perpendicular to a long straight coast. The resulting sea will be termed "abnormally" or "subnormally developed".

The experiments of Snyder and Cox (1966), Barnett and Wilkerson (1967), and K. Hasselmann *et al.*, (1972), are cases of "normal development"; those of Dobson (1971), Elliott (1972), and the present experiments are cases of "subnormal development".

In the first case, the spectrum of surface elevation is parameterized by the nondimensional fetch $\tilde{x}$ and is self similar. Over the range $\tilde{x} = 10^2$ to $10^4$, the spectrum is of the approximate form (3), and the spectral parameters $\varepsilon$, $\tilde{\Omega}$, $\gamma$, $\sigma$, and $\tilde{\mathscr{e}}$, where

$$\tilde{\mathscr{e}} \equiv \frac{g^2}{W^4} \int\limits_0^\infty d\omega\, G_{\zeta^2}(\omega),$$

are proportional to powers of $\tilde{x}$:

$$\varepsilon \doteq .57\, \tilde{x}^{-1/2},$$

$$\tilde{\Omega} \doteq 22.\, \tilde{x}^{-1/3},$$

$$\gamma \doteq 3.3,$$

$$\sigma \doteq .09,$$

and

$$\tilde{\mathscr{e}} \doteq 5.0 \times 10^{-7}\tilde{x}^{5/6}.$$

The power laws chosen here differ from those chosen by K. Hasselmann *et al.* (1973), but are consistent with the JONSWAP data. A second choice with $\varepsilon \sim \tilde{x}^{-1/3}$ and $\tilde{\mathscr{e}} \sim \tilde{x}$ preserves similarity but does not appear to fit the JONSWAP data as well. (This scaling leads to conclusions similar to those which follow.) The JONSWAP choice, $\varepsilon \sim \tilde{x}^{-.22}$ and $\tilde{\mathscr{e}} \sim \tilde{x}$, allows additional low fetch data to fit into the general pattern, but as remarked by K. Hasselmann *et al.*, does not fit the JONSWAP data particularly well.

In the second case, it appears from the May 1970 BOA data that there may exist a subclass of "subnormally developed" seas for which the same spectral form and the same power laws obtain except that $\varepsilon$ and $\tilde{\mathscr{e}}$ are proportionately smaller.

In both cases, the atmospheric input of energy and momentum are controlled by the growth rate parameter $\beta$. In three separate field experiments, $\beta$ has been measured to be of the approximate form

$$\beta \doteq \mu s(\boldsymbol{k} \cdot \boldsymbol{W} - \omega(k)), \tag{6}$$

where $s$ is the ratio of the density of air to that of water and $\mu$ is a numerical coefficient found to be $\sim 1$. (Dobson), $\sim .2$ (Elliott), and $\sim .1$ (present experiments). As an explanation for the discrepancy in the value of $\mu$, there appear to be several possibilities:

1) At least one, and perhaps all three, of the measurements are wrong.
2) The mean atmospheric fields controlling the atmospheric interaction (the velocity profile being probably the most important), differ sufficiently to account for the discrepancy. It seems possible that this explanation might readily account for the difference between the present measurements and those of Elliott (note the systematic difference between the May 1970 and April 1972 BOA measurements); however, it is unlikely that this explanation can readily account for the difference between these measurements and those of Dobson.
3) The profile of wave-induced atmospheric pressure does not extrapolate to the mean surface in exponential fashion as assumed by both Elliott and the present study. The tendency for the amplitude data of Figure 8 to be larger than the prediction of linear potential theory for small kz supports this explanation; however, the observed tendency is not necessarily significant.

A proper resolution of these discrepancies would seem to involve further field experiments designed to look more carefully at the profile of wave-induced atmospheric pressure.

Relation (6) and the spectral form (3) may be used to estimate the energy and momentum transfer from the atmosphere to the wave field. (This estimate involves a fairly extensive extrapolation at higher frequencies.) Here, only the integral momentum transfer will be examined. This transfer is conveniently cast in terms of a drag coefficient $C_{IN}$ which, assuming a $\cos^2\theta$ spreading, can be shown to be of the form

$$C_{IN} \simeq \frac{3}{4}\mu\varepsilon\tilde{\Omega}^{-1}I_2 - \frac{8}{3\pi}\mu\varepsilon\tilde{\Omega}^{-2}I_3, \tag{7}$$

where

$$I_2(\gamma,\sigma) \equiv \int_0^\infty d\lambda\,\lambda^{-2}e^{-5/4\lambda^{-4}}\gamma e^{-\frac{(\lambda-1)^2}{2\sigma^2}}$$

and

$$I_3(\gamma,\sigma) \equiv \int_0^\infty d\lambda\,\lambda^{-3}e^{-5/4\lambda^{-4}}\gamma e^{-\frac{(\lambda-1)^2}{2\sigma^2}}.$$

Numerical integration gives $I_2(3.3, .09) \simeq .88$ and $I_3(3.3, .09) \simeq .51$. Relation (7) is plotted in Figure 19 for a "normally developed" sea using the power laws (5). The drag coefficients $C_{AD} \simeq 3/8\,s^{-1}d\tilde{\mathscr{E}}/d\tilde{x}$, representing the momentum

advected away by the wave field, $C_{HF}$ $\simeq .17\, s^{-1}\varepsilon^3\tilde{\Omega}^{-2}$, representing the momentum transferred to high frequencies by the nonlinear transfer mechanism, $C_{DS} \equiv C_{AD} - C_{IN}$, representing the momentum dissipated, and the linear combinations $C_{AD} + C_{HF}$ and $C_{HF} + C_{DS}$ are also plotted. The relations for $C_{AD}$ and $C_{HF}$ are taken directly from K. Hasselmann *et al.* The drag coefficients are plotted for $\mu = 1., .2, .1,$ and $.05$.

It is seen that in all four cases $C_{IN} > C_{AD}$, indicating that the atmospheric input is adequate to provide the momentum advected away by the wave field. K. Hasselmann *et al.* suggest, however, that a more appropriate lower limit on the necessary drag coefficient $C_{IN}$ (assuming (1) that the momentum transferred to high frequencies is absorbed primarily by dissipation, and (2) that the momentum dissipated in the main part of the spectrum is small) is given by the sum $C_{AD} + C_{HF}$. Note that for all $\mu$ represented



Figure 19. Fetch dependence of various drag coefficients.

$$+ - C_{IN}$$
$$O - C_{AD}$$
$$X - C_{HF}$$
$$\Delta - C_{DS} = C_{AD} - C_{IN}$$
$$\Diamond - C_{AD} + C_{HF}$$
$$Y - C_{HF} + C_{DS}$$

$$C_{IN} \geq C_{AD} + C_{HF}$$

in the range $\tilde{x} = 10^3$ to $10^4$ with

$$C_{IN} \simeq C_{AD} + C_{HF} \quad (\text{i.e. } C_{DS} + C_{HF} \simeq 0)$$

in this range for $\mu = .05$.

There are two break points in the plots where physical constraints imply that the assumed fetch dependences must change. The upper break point occurs at $\tilde{x} \simeq 3.5 \times 10^4$. Here $C_{IN} \simeq 0$, implying a balance between the momentum provided by the atmosphere at high frequencies and the momentum absorbed by the atmosphere at low frequencies. While the calculation is somewhat schematic (It assumes that relation (6) can be extrapolated to wave components for which $\boldsymbol{k} \cdot \boldsymbol{W} < \omega(k)$), nonetheless it probably identifies with reasonable precision the largest value of the nondimensional fetch for which the assumed power laws can hold. Presumably, beyond $\tilde{x}^2 \simeq 10^4$, $\gamma \to 1.$, and $\varepsilon$ and $\tilde{\Omega}$ approach the Pierson-Moskowitz (1964) values.
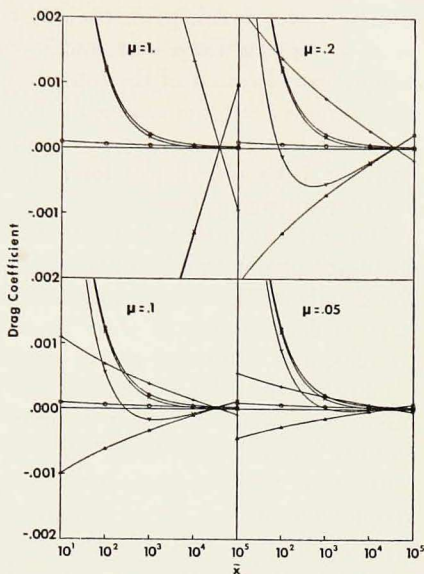
The lower break point occurs at $\tilde{x} \simeq 2 \times 10^4$ for $\mu = 1.$, $\tilde{x} = 3 \times 10^3$ for $\mu = .2$, $\tilde{x} = 4 \times 10^2$ for $\mu = .1$, and $\tilde{x} = 1.5 \times 10^2$ for $\mu = .05$. Here, $C_{IN} \sim .0005$, a significant fraction of the total drag coefficient. Clearly, the atmospheric input cannot sustain the assumed power laws much below the lower break point. It should be noted that for $\mu = .1$ or $.2$, both break points are quite consistent with the JONSWAP plot for $\varepsilon$. For $\mu = 1.$, the lower break point is inconsistent with this plot.

The presence of break points related to the atmospheric input suggests that the development of a "normal" sea probably occurs in several stages in which the details of the energy and momentum balance differ. In the "principal" stage of development ($\tilde{x} = 10^2$ to $10^4$), the atmospheric interaction, nonlinear transfer, and dissipation are all significant, with nonlinear transfer playing an increasingly less significant role as $\tilde{x}$ increases. All three mechanisms involve momentum transfers which decrease with $\tilde{x}$. The principal stage of development is followed by a "final" stage of development, in which the spectrum approaches an equilibrium maintained by a balance between the atmospheric interaction (now with a $(- +)$ signature), dissipation, and nonlinear transfer, and is preceded by an "initial" stage of development during the latter part of which the atmospheric interaction may in fact be saturated (A large part of the total stress is transferred to the wave field.), and in which nonlinear transfer undoubtedly plays a significant if not dominant role.

The integral momentum balance for the "subnormally" developed sea present in the May 1970 BOA experiment would be expected to differ from that for a "normally" developed sea in the following respects:

1) $C_{IN}$, $C_{AD}$, and $C_{DS}$ will be approximately one-half as large,
2) $C_{HF}$ will be approximately one-sixth as large, and thus
3) Nonlinear transfer will not play as important a role as in the case of a "normally" developed sea.

With respect to the growth of a particular wave component, K. Hasselmann *et al.* show that for JONSWAP scaling the nonlinear energy transfer to components on the low frequency face of the spectrum can account for the observed growth of these components in the case of "normally" developed seas. Presumably this conclusion applies to the scaling (5) as well. In the case of "subnormally" developed seas, however, the growth of low frequency components apparently proceeds at a somewhat slower rate, with nonlinear transfer and the atmospheric interaction both contributing significantly to this growth.

## 10. Conclusions

1.   In the frequency range .1 to 5 rad/s, the atmospheric pressure field close to the water surface is dominated by two components: turbulent fluctuations and surface gravity waves.

2. The corresponding spectrum typically exhibits a large wave-induced peak superimposed on a monotonically decreasing (turbulent) background.

3. The turbulent component has the dispersion of "frozen" turbulence.

4. The surface gravity wave component is, on occasion, dominated by upwind-traveling waves as a result of dynamic amplification of these waves (relative to downwind-traveling waves) in the atmospheric pressure field.

5. In the experiments described, most, but not all, observations of upwind-traveling surface gravity waves can be explained as a result of reflections from the laboratory vessel.

6. The data support the conclusion that the wave-coherent part of the atmospheric pressure field decays exponentially without change of phase from the mean surface. The decay parameter is essentially that predicted by linear potential theory.

7. The wave-coherent part of the atmospheric pressure field is comparable with the predictions of the Miles (1957) theory. Discrepancies between observation and theory may or may not be significant.

8. The implied growth rates are not adequate to account for the growth of surface gravity waves observed by Snyder and Cox (1966), Barnett and Wilkerson (1967), and others.

9. This conclusion (8.) is consistent with the conclusion of K. Hasselmann *et al.* (1973): In a "normally" developing sea, waves on the low frequency face of the spectrum grow primarily as a result of nonlinear interactions.

10. The energy and momentum transfer to the wave field are largest for frequencies near the peak of the wave spectrum. (The transfer peak is displaced somewhat to higher frequency.)

11. In the BOA experiments, the observed net momentum transfer to waves near the spectral peak was approximately 2% of the wind stress estimated from profile measurements.

12. Analysis of the directional cross-spectrum between atmospheric pressure and surface elevation indicates that: (a) waves traveling against the wind are damped (for $\mathbf{k} \cdot \mathbf{W}/\omega < -2$ they may be amplified), and (b) waves traveling faster than the wind may also be damped.

13. The wave spectra for May 1970 are consistent with the similarity model of K. Hasselmann *et al.*, except that the Phillips (1958) parameter is approximately one-half as large.

14. This lowering of the Phillips parameter is probably the result of the some-what different fetch distribution.

15. The implied nonlinear transfer for the May 1970 BOA spectra is roughly one-sixth that of JONSWAP.

16. The integral momentum transfer from the atmosphere to the JONSWAP wave field estimated from the present study is consistent with the overall momentum balance as discussed by K. Hasselmann *et al.* (1973). This transfer is smaller than the total stress, but is adequate to provide the momentum required by the evolving wave field.

17. The estimated integral momentum transfer may account for several features of the JONSWAP plot of the Phillips parameter.

## REFERENCES

BARNETT, T. P., and J. C. WILKERSON
  1967. On the generation of wind waves as inferred from airborne radar measurements of fetch-limited spectra. J. Mar. Res., *25*: 292–328.

BARTLETT, M. S.
  1950. Periodogram analysis and continuous spectra. Brometrika, *37*: 1–16.

DOBSON, F. W.
  1971. Measurements of atmospheric pressure on wind-generated sea waves. J. Fluid Mech., *48*: 91–127.

ELLIOTT, J. A.
  1972. Microscale pressure fluctuations near waves being generated by wind. J. Fluid Mech., *54*: 427–448.

GILCHRIST, A. W. R.
  1966. The directional spectrum of ocean waves: an experimental investigation of certain predictions of the Miles-Phillips theory of wave generation. J. Fluid Mech., *25*: 795–816.

HASSELMANN, K.
  1960. Grundleichungen der Seegangsvoraussage. Shiffstechnik, *7*: 191–195.

1962. On the non-linear energy transfer in a gravity-wave spectrum. I. General Theory. J. Fluid Mech., *12*: 481–500.

1963. On the non-linear energy transfer in a gravity-wave spectrum. Part 3. J. Fluid Mech., *15*: 385–398.

1966. Feynman diagrams and interaction rules of wave-scattering processes. Rev. Geophys., *4*: 1–32.

HASSELMANN, K., BARNETT, T. P., E. BOUWS, H. CARLSON, D. E. CARTWRIGHT, K. ENKE, J. A. EWING, H. GIENAPP, D. E. HASSELMANN, P. KRUSEMANN, A. MEERBURG, P. MÜLLER, D. J. OLBERS, K. RICHTER, W. SELL, and H. WALDEN

1973. Measurements of wind-wave growth and swell decay during the Joint North Sea Wave Project (JONSWAP). Ergänzungsheft zur Deutschen Hydrographischen Zeitschrift, Reihe A (8°), Nr. 12.

LONG, R. B.

1971. On generation of ocean waves by a turbulent wind. Ph. D. Dissertation, University of Miami, Miami, Florida. 193 pp.

1973. Scattering of surface waves by an irregular bottom. J. Geophys. Res., *78*(33): 7861–7870.

LONGUETT-HIGGINS, M. S., D. E. CARTWRIGHT, and N. D. SMITH

1963. Observations of the directional spectrum of sea waves using the motions of a floating buoy. *In* Ocean wave spectra, pp. 111–132. Proceedings of a conference, Easton, Md., May 1–4, 1961. Prentice-Hall, Inc., Englewood Cliffs, N.J. 357 pp.

MILES, J. W.

1957. On the generation of surface waves by shear flows. J. Fluid Mech., *3*: 185–204.

PHILLIPS, O. M.

1957. On the generation of waves by turbulent wind. J. Fluid Mech., *2*: 417–445.

1958. The equilibrium range in the spectrum of wind-generated ocean waves. J. Fluid Mech., *4*: 426–434.

PIERSON, W. J., and L. MOSKOWITZ

1964. A proposed spectral form for fully developed wind seas based on the similarity theory of S. A. Kitaigorodskii. J. Geophys. Res., *69*: 5181–5190.

PRIESTLEY, J. T.

1965. Correlation studies of pressure fluctuations on the ground beneath a turbulent boundary layer. Nat. Bur. Stand. Rep., 8942, 92 pp.

SHEMDIN, O.

1969. Instantaneous velocity and pressure measurements above propagating waves. Univ. Florida Dept. Coastal and Oceanographic Engineering, Rep., 4, 105 pp.

SNYDER, R. L.

1973. Covariance equations for a linear sea. J. Mar. Res., *31*: 40–50.

SNYDER, R. L., and C. S. COX

1966. A field study of the wind generation of ocean waves. J. Mar. Res., *24*: 141–178.

SNYDER, R. L., R. B. LONG, J. IRISH, D. G. HUNLEY, and N. C. PFLAUM

1973. An instrument to measure atmospheric pressure fluctuations above surface gravity waves. To be published.